VIP Heterogeneous Catalysis Very Important Paper

International Edition: DOI: 10.1002/anie.201709723
German Edition: DOI: 10.1002/ange.201709723

Integrated Transmission Electron and Single-Molecule Fluorescence Microscopy Correlates Reactivity with Ultrastructure in a Single Catalyst Particle

Frank C. Hendriks[+], Sajjad Mohammadian[+], Zoran Ristanović, Sam Kalirai, Florian Meirer, Eelco T. C. Vogt, Pieter C. A. Bruijnincx, Hans C. Gerritsen, and Bert M. Weckhuysen**

Abstract: *Establishing structure–activity relationships in complex, hierarchically structured nanomaterials, such as fluid catalytic cracking (FCC) catalysts, requires characterization with complementary, correlated analysis techniques. An integrated setup has been developed to perform transmission electron microscopy (TEM) and single-molecule fluorescence (SMF) microscopy on such nanostructured samples. Correlated structure–reactivity information was obtained for 100 nm thin, microtomed sections of a single FCC catalyst particle using this novel SMF-TEM high-resolution combination. High reactivity in a thiophene oligomerization probe reaction correlated well with TEM-derived zeolite locations, while matrix components, such as clay and amorphous binder material, were found not to display activity. Differences in fluorescence intensity were also observed within and between distinct zeolite aggregate domains, indicating that not all zeolite domains are equally active.*

Fluid catalytic cracking (FCC) is among the most important oil refining processes, converting heavier oil fractions into lighter, more desirable products, such as gasoline and LPG.[1,2] The FCC catalyst used is a typical example of a complex, hierarchically structured nanomaterial, consisting of a mixture of zeolite, clay, alumina and other binder materials, which differ in their chemical (e.g., acidity) and structural properties (e.g., porosity).[3,4] High-resolution micro-spectroscopy methods have been developed to study structure and activity[5,6] as well as deactivation[7–9] of such industrially relevant catalyst particles, providing insight into intra- and interparticle heterogeneities. For example, the ratio of tetrahedral versus octahedral Al in the active zeolite components of FCC catalyst particles was found to vary, suggesting heterogeneities in Brønsted acidity within individual catalyst particles.[10] Furthermore, deactivation mechanisms, such as dealumination and lattice destruction of the zeolite phase by steaming[10,11] and pore blockage by metal deposition,[6,9] occur simultaneously, bringing about structural as well as chemical changes within the catalyst material during operation. Given the complexity of both the material and its deactivation mechanisms, FCC particle studies, or in general any complex functional material, require a combination of techniques, preferably correlated, to provide a thorough understanding of structure-performance relations. Additionally, these correlated techniques should both have high resolution, as nanoscale heterogeneities are present in the material. Such knowledge can then ultimately serve to guide rational design of solid catalysts.

Obtaining correlated spatiotemporally resolved information from different characterization techniques on the same sample presents several technical challenges. Integration of different techniques in one instrument can facilitate this. The combination of fluorescence and electron microscopy is a well-known example; originally pioneered in the life sciences,[12] this technique has recently also made its way into materials science.[13,14] Indeed, fluorescence microscopy (FM) is an effective tool to study reactivity and diffusion in catalytic materials,[15–18] while electron microscopy (EM) can visualize the different ultrastructures present. For example, confocal FM of whole FCC catalyst particles after Brønsted acid sites staining by styrene or thiophene oligomerization[19] has been combined with transmission electron microscopy (TEM) to correlate structure degradation with reactivity loss.[13,14] Excitingly, FM has now improved beyond the traditionally diffraction-limited resolution of light microscopy, bringing sensitivity and resolution to the level of individual molecules.[20,21] Single-molecule fluorescence (SMF) microscopy has indeed been used to study catalytic turnovers on individual active sites of catalyst particles.[5,22] Very recently, SMF was combined with scanning electron microscopy (SEM) to study photocatalysis over ZnO crystals and the acidity of mordenite crystals.[23,24]

[*] F. C. Hendriks,[+] Dr. Z. Ristanović, Dr. S. Kalirai, Dr. F. Meirer, Prof. Dr. E. T. C. Vogt, Dr. P. C. A. Bruijnincx, Prof. Dr. B. M. Weckhuysen
Inorganic Chemistry and Catalysis
Debye Institute of Nanomaterials Science
Utrecht University
Universiteitsweg 99, 3584 CG Utrecht (The Netherlands)
E-mail: b.m.weckhuysen@uu.nl

S. Mohammadian,[+] Prof. Dr. H. C. Gerritsen
Molecular Biophysics
Department of Soft Condensed Matter and Biophysics
Science Faculty, Utrecht University
Princetonplein 1, 3584 CC Utrecht (The Netherlands)
E-mail: h.c.gerritsen@uu.nl

[+] These authors contributed equally to this work.

Supporting information and the ORCID identification number(s) for the author(s) of this article can be found under: https://doi.org/10.1002/anie.201709723.

To the best of our knowledge, high-resolution localization of reactive sites using SMF has not yet been combined with detailed structural TEM analysis of single catalyst particles. Here, we for the first time demonstrate such a correlative SMF-TEM analysis to identify and correlate reactivity and ultrastructure within an individual ZSM-5-containing FCC particle. An integrated setup, with a FM module built into a TEM machine, allowed both techniques to be applied in a single experiment and on one sample (see Figure S1 in the Supporting Information). An overview of the developed approach is shown in Figure 1. TEM measurements demand a very thin sample on an electron-transparent substrate and SMF requires an extremely low fluorescent background. A fresh FCC catalyst particle was embedded in an epoxy resin matching the hardness of the catalyst particles and microtomed into 100 nm thin sections (Figure 1 a). The thin sections were placed on heat-resistant silicon nitride (SiN) membranes coated with TiO_2 to prevent any interaction of the catalyst with the SiN membrane. Calcination at high temperature removed the resin and any organic impurities, leaving just the catalyst thin sections on the coated SiN (Figure 1 b and S2). The TEM image of the thin section shows the catalyst to be in good shape after this procedure, even though few cutting artifacts perpendicular to the cutting direction (from top right to bottom left) do exist (Figure 1 c).

Thiophene oligomerization was used as a sensitive single-molecule probe reaction, generating fluorescent species that allow the active acid sites in the catalyst thin section to be visualized (Figure 1 d).[19,25] Both SMF and TEM measurements were carried out in the vacuum chamber of the integrated setup; therefore, thiophene was deposited directly onto the sample prior to insertion. A 46 min movie was recorded (Figure 1 d and movie S1) and fluorescence can be observed as bright, high-intensity events for the full duration of the experiment (Figure S3), suggesting that adsorption of reactants and subsequent product formation, most probably in the micropores of zeolite ZSM-5, was sufficient to observe catalytic events, even under the high vacuum conditions. Notably, a 532 nm laser was used as it most effectively excites higher, less volatile oligomer products, that is, mostly trimeric species or larger.[26] Thus, a pool of dimerized and adsorbed thiophene species may form, which further oligomerize to species that can be excited by the laser.

Fluorescence intensity was evaluated using two complementary super-resolution techniques: Nanometer Accuracy by Stochastic Chemical reactions (NASCA)[27,28] and Super-resolution optical fluctuation imaging (SOFI).[29] Both techniques rely on stochastic and reversible fluorescent fluctuations, here caused by excitation and immediate photobleaching of fluorescent molecules being continuously formed on the Brønsted acid sites in the FCC particle.[5] NASCA detects high intensity, single catalytic turnovers, such as those seen in Figure 1 d; these events are localized by fitting a 2D Gaussian to the fluorescence intensity to give a resolution of 25 nm

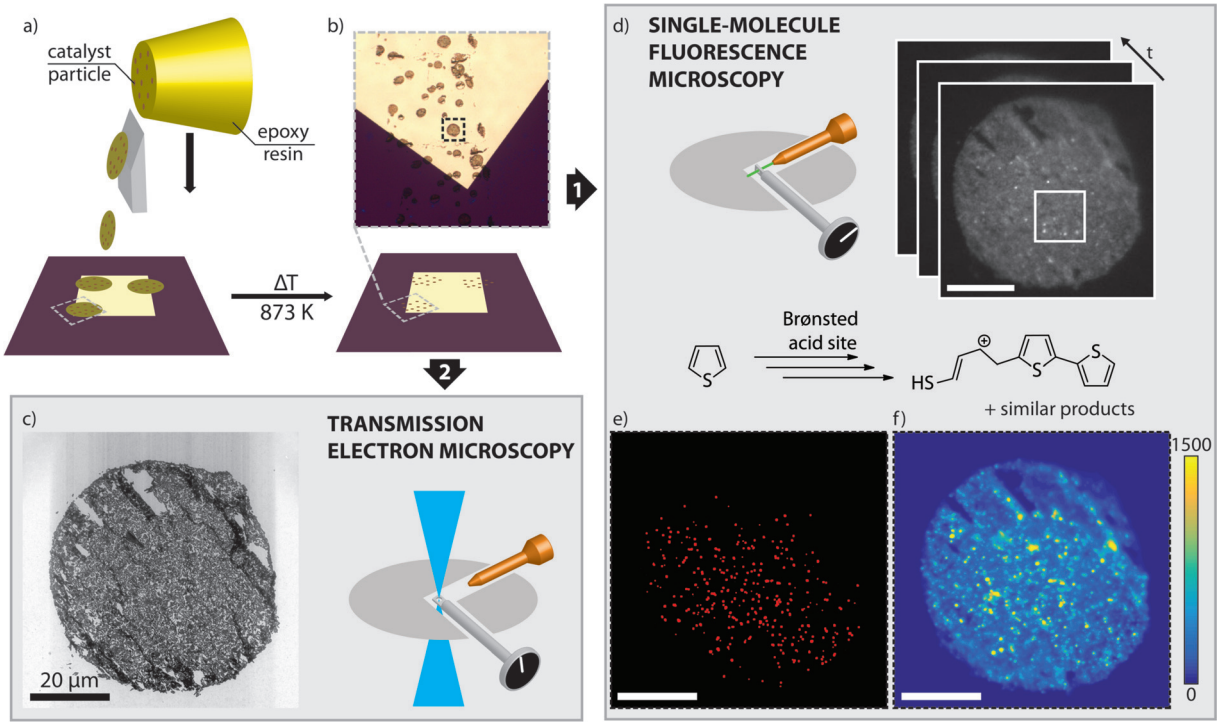

Figure 1. Integrated SMF microscopy and TEM of a single catalyst particle. a) Fluid catalytic cracking (FCC) particles embedded in epoxy resin (yellow) are microtomed into thin sections and deposited onto a SiN membrane. b) Calcination of the SiN membrane removes the resin, leaving just the catalyst thin sections. c) TEM image of the thin section. d) Sample reactivity is evaluated by SMF using the thiophene oligomerization as probe reaction; a movie with 9200 frames is recorded (Movie S1), showing the emitted fluorescence as bright, diffraction-limited spots. The movie is analyzed by NASCA (e) and SOFI (f). e) Map of detected single-molecule events by NASCA. For clarity, the detected events have been enlarged. Fewer events are observed in the top right area because it is slightly out of focus. f) Map of the SOFI intensity. The scale bars represent 20 µm.

(Figure S4). NASCA analysis requires a high signal-to-noise ratio (SNR) and long experiment duration, so that enough single catalytic turnovers are recorded. A map of all the events detected by NASCA is shown in Figure 1e. Conversely, SOFI analyzes temporal fluctuations in fluorescence in each pixel separately using higher-order statistics. This way, SOFI analysis can increase the resolution, while simultaneously eliminating (non-fluctuating) background fluorescence. Indeed, the ample background fluorescence (e.g. in Figure 1d, the wide-field movie frames show a low, static fluorescence signal over the complete thin section) observed in the movie is effectively suppressed by SOFI. The resulting SOFI intensity image for the complete thin section is shown in Figure 1f. To correlate reactivity with (ultra)structure, the NASCA, SOFI and TEM results were overlaid based on features visible in both FM and TEM, using a combination of automatic and manual correlation (Figure S5).

Secondly, catalyst structure was studied at high resolution using TEM (Figure 2a and b). TEM images at intermediate and high magnification show the structural features of the FCC catalyst. Zeolite crystals fragmented by the cutting procedure (I), relatively intact zeolite crystals (II) and non-zeolitic matrix elements (III) are highlighted in Figure 2b, in line with previous studies.[13,14,30,31] The clay, silica and alumina matrix elements could not be separately identified. Next, these zoomed-in TEM images were compared to co-localized fluorescence intensity events. A combination of NASCA events and SOFI intensity at the same locations as the intermediate and high magnification TEM images (Figure 2a and b) is shown in Figure 2c and d. Both NASCA and SOFI images show highly localized regions of fluorescence, and the overlay of the two super-resolution techniques shows they are highly correlated. A few areas with many NASCA events show no SOFI intensity; these are most likely caused by non-fluctuating contaminant species (see supporting information). The combination of NASCA and SOFI allows detection of these species and therefore shows the value of employing both types of analysis.[5] Conversely, areas are found with only SOFI intensity and no NASCA events. These areas demonstrate the higher sensitivity of SOFI to detect fluorescence compared to NASCA. The obtained SOFI intensity maps show more subtle differences in reactivity, albeit with a lower spatial resolution than NASCA, and show that an absence of detected fluorescence by NASCA does not necessarily mean there is no activity in a region.

The power of the TEM-SMF approach is demonstrated by a combination of the NASCA, SOFI and TEM results (Figure 2e and f). The TEM images are thresholded and overlaid on the SOFI images, with NASCA on top of both of these. Areas with high NASCA and SOFI intensity clearly coincide with the areas in TEM containing structural features I and II. This correlation of fluorescence activity with the active phase of the catalyst validates both our staining procedure as well as the image correlation. However, the correlation of NASCA and SOFI with TEM also shows that certain zeolite domains do not seem to show any activity, even

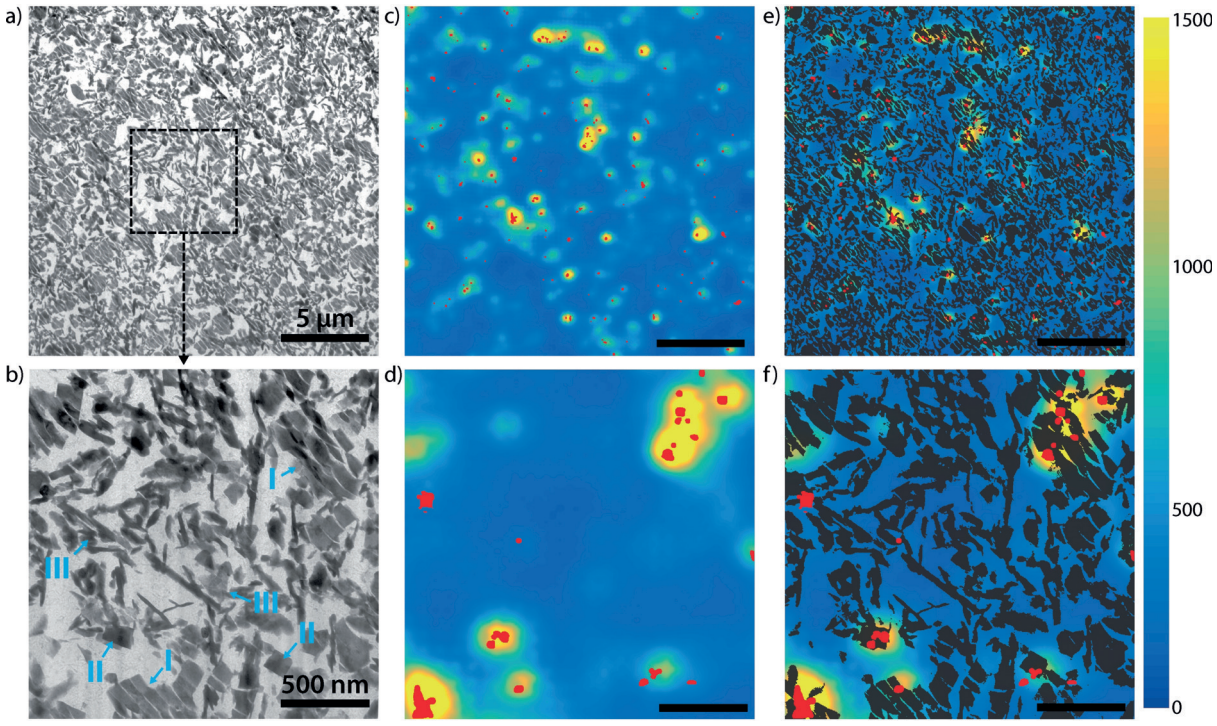

Figure 2. Analysis of SMF and TEM and overlays of an intermediate zoom level (a, c, e, all showing the same area) and high zoom level (b, d, f, all showing the same area) of the thin section. The intermediate zoom level is marked by a white square in Figure 1c. The high zoom level area is marked in a. a,b) TEM of the catalyst thin section. In b), different types of ultrastructure are marked: fragmented zeolites (I); intact zeolite crystals (II); non-zeolitic matrix material (III). c,d) Combined maps of NASCA and SOFI intensity (NASCA events in red and SOFI intensity corresponding to the scale bar). e,f) Thresholded TEM images (a and b), showing the structure, overlaid on the NASCA/SOFI images from (c) and (d). Scale bars represent 5 µm (a,c,e) or 500 nm (b,d,f).

though the underlying TEM structures look similar to domains that do show intensity. For NASCA it can be argued only the most active zeolite domains show single catalytic turnovers, but SOFI should be sensitive to low fluorescence intensity. Thus, the correlative analysis indicates that intrinsic differences in reactivity exist among zeolite aggregates of seemingly identical structure. Additionally, Figure 2 f shows differences in reactivity even within one zeolite domain. These differences have been observed before in similar fluorescence staining experiments of FCC particles, but the unique correlative approach presented here allows us now to unambiguously link reactivity to ultrastructure.[5,19] The differences seen in reactivity may be explained by differences in the distribution of Al coordination in the zeolite particles, which has been shown to vary within ZSM-5 particles[32] as well as in zeolite Y embedded in FCC catalysts.[10] Furthermore, previous research has shown polarization dependence of the fluorescent products can also play a role in ZSM-5 containing FCC particles, although this does not apply to reactivity differences within one zeolite domain.[33] Differences in accessibility within the catalyst particle can be excluded, as the thiophene reaction is carried out after microtoming, eliminating accessibility gradients.

The correlation between SOFI intensity and structural features was further explored. To gain more quantitative information, a region of interest (ROI) within a catalyst thin section of $20 \times 20\ \mu m^2$ was divided into sections of $0.5 \times 0.5\ \mu m^2$ (Figure 3 a). The dominant structural feature of each square was then manually classified into zeolite material (type I and II in Figure 2 b) and non-zeolitic matrix material (type III in Figure 2 b). It must be emphasized here that this classification was based solely on structural information in the TEM, that is, not on the corresponding SOFI intensity of these squares. The zeolite material was found to be homogeneously distributed in this ROI, covering 38 % of the surface of the thin section. A further 46 % was covered by matrix material, while 16 % contained no material. Consequently, the SOFI intensity of each of these types was evaluated as a measure of reactivity (Figure 3 b). A significant higher reactivity was found for the zeolite compared to the matrix material, showing that the probe reaction used most effectively stains zeolite material with strong Brønsted acid sites within the catalyst. Furthermore, the majority of matrix material showed similar reactivity to areas with no material present, suggesting this is mostly background fluorescence. The observed heterogeneity in fluorescence intensity for each type is partly caused by the resolution of the classification map, as the squares in Figure 3 a can contain more than 1 type of material. However, as observed in Figure 2, the observed heterogeneity in fluorescence intensity for zeolite material again shows differences in activity for zeolite particles with identical structural features. Conversely, an alternative approach, in which the TEM image was segmented based on the observed SOFI intensity using a thresholding procedure, showed similar results (Figure S6).

In summary, a generally applicable, correlated microspectroscopy approach with nanoscale spatial resolution is presented, which combines transmission electron microscopy (TEM) and single-molecule fluorescence (SMF) microscopy.

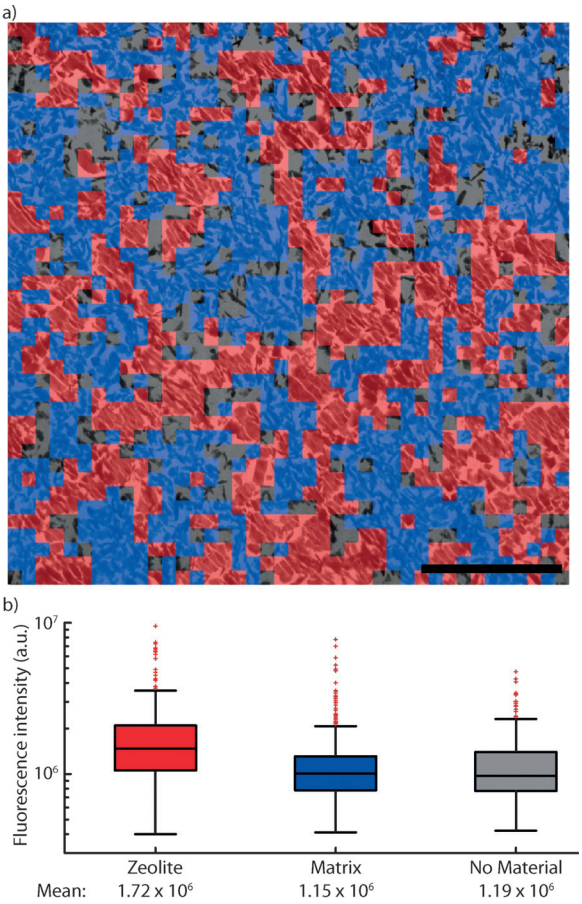

Figure 3. a) A zoomed-in area of the TEM image (same image as Figure 2 a), with each structural element classified as either zeolite (604 squares, 38 %), matrix (739 squares, 46 %) or with no material present (260 squares, 16 %). Each square represents an area of $0.5 \times 0.5\ \mu m^2$; the scale bar represents 5 µm. b) Box plots of the SOFI intensity in the areas of each type of material classified. The whiskers represent the data within 2.7σ; other points are considered outliers (red squares), but are still used to calculate the mean.

The utility of this integrated SMF-TEM approach has been demonstrated by its application to a single fluid catalytic cracking (FCC) particle, correlating for the first time ultrastructures, such as zeolite, clay and binder with (lack of) reactivity. Clear differences in reactivity were observed between the active zeolite phase and the non-zeolitic matrix components. It is shown that among the zeolite aggregate domains with seemingly identical structural features significant differences in reactivity exist. It is our opinion that the developed SMF-TEM combination can aid in elucidating structure-performance relationships for a wide range of functional materials, such as other solid catalysts, batteries, adsorbents and fuel cells.

Acknowledgements

We thank Albemarle for providing the FCC catalyst, J. van Gerwen (Eindhoven University of Technology) is acknowledged for performing atomic layer deposition

(ALD) and J. D. Meeldijk (Utrecht University) for FCC thin sectioning. BMW acknowledges the Netherlands Organization for Scientific Research (NWO) for a Top research grant and the European Research Council (ERC) for an Advanced Grant (number 321140). HCG acknowledges the Microscopy Valley programme, sponsored by Toegepaste en Technische Wetenschappen (TTW) of NWO (project number 12713).

Conflict of interest

The authors declare no conflict of interest.

Keywords: electron microscopy · heterogeneous catalysis · single-molecule microscopy · structure–activity relationships · zeolites

How to cite: *Angew. Chem. Int. Ed.* **2018**, *57*, 257–261
Angew. Chem. **2018**, *130*, 263–267

[1] J. H. Gary, G. E. Handwerk, M. J. Kaiser, in *Petroleum Refining: Technology and Economics*, CRC, New York, **2007**, p. 115.
[2] E. T. C. Vogt, B. M. Weckhuysen, *Chem. Soc. Rev.* **2015**, *44*, 7342–7370.
[3] C. Perego, R. Millini, *Chem. Soc. Rev.* **2013**, *42*, 3956–3976.
[4] C. Martínez, A. Corma, *Coord. Chem. Rev.* **2011**, *255*, 1558–1580.
[5] Z. Ristanović, M. M. Kerssens, A. V. Kubarev, F. C. Hendriks, P. Dedecker, J. Hofkens, M. B. J. Roeffaers, B. M. Weckhuysen, *Angew. Chem. Int. Ed.* **2015**, *54*, 1836–1840; *Angew. Chem.* **2015**, *127*, 1856–1860.
[6] J. C. da Silva, K. Mader, M. Holler, D. Haberthür, A. Diaz, M. Guizar-Sicairos, W.-C. Cheng, Y. Shu, J. Raabe, A. Menzel, et al., *ChemCatChem* **2015**, *7*, 413–416.
[7] F. Meirer, S. Kalirai, D. Morris, S. Soparawalla, Y. Liu, G. Mesu, J. C. Andrews, B. M. Weckhuysen, *Sci. Adv.* **2015**, *1*, e1400199.
[8] Á. Ibarra, A. Veloso, J. Bilbao, J. M. Arandes, P. Castaño, *Appl. Catal. B* **2016**, *182*, 336–346.
[9] Y. Liu, F. Meirer, C. M. Krest, S. Webb, B. M. Weckhuysen, *Nat. Commun.* **2016**, *7*, 12634.
[10] S. Kalirai, P. P. Paalanen, J. Wang, F. Meirer, B. M. Weckhuysen, *Angew. Chem. Int. Ed.* **2016**, *55*, 11134–11138; *Angew. Chem.* **2016**, *128*, 11300–11304.
[11] G. Agostini, C. Lamberti, L. Palin, M. Milanesio, N. Danilina, B. Xu, M. Janousch, J. A. van Bokhoven, *J. Am. Chem. Soc.* **2010**, *132*, 667–678.
[12] A. V. Agronskaia, J. A. Valentijn, L. F. van Driel, C. T. W. M. Schneijdenberg, B. M. Humbel, P. M. P. van Bergen en Henegouwen, A. J. Verkleij, A. J. Koster, H. C. Gerritsen, *J. Struct. Biol.* **2008**, *164*, 183–189.
[13] M. A. Karreman, I. L. C. Buurmans, J. W. Geus, A. V. Agronskaia, J. Ruiz-Martínez, H. C. Gerritsen, B. M. Weckhuysen, *Angew. Chem. Int. Ed.* **2012**, *51*, 1428–1431; *Angew. Chem.* **2012**, *124*, 1457–1460.
[14] M. A. Karreman, I. L. C. Buurmans, A. V. Agronskaia, J. W. Geus, H. C. Gerritsen, B. M. Weckhuysen, *Chem. Eur. J.* **2013**, *19*, 3846–3859.
[15] J. Michaelis, C. Bräuchle, *Chem. Soc. Rev.* **2010**, *39*, 4731–4740.
[16] P. Chen, X. Zhou, N. M. Andoy, K.-S. Han, E. Choudhary, N. Zou, G. Chen, H. Shen, *Chem. Soc. Rev.* **2014**, *43*, 1107–1117.
[17] K. P. F. Janssen, G. De Cremer, R. K. Neely, A. V. Kubarev, J. Van Loon, J. A. Martens, D. E. De Vos, M. B. J. Roeffaers, J. Hofkens, *Chem. Soc. Rev.* **2014**, *43*, 990–1006.
[18] K. Kitagawa, S. A. Blum, *ACS Catal.* **2017**, *7*, 3786–3791.
[19] I. L. C. Buurmans, J. Ruiz-Martínez, W. V. Knowles, D. van der Beek, J. A. Bergwerff, E. T. C. Vogt, B. M. Weckhuysen, *Nat. Chem.* **2011**, *3*, 862–867.
[20] F. C. Hendriks, F. Meirer, A. V. Kubarev, Z. Ristanović, M. B. J. Roeffaers, E. T. C. Vogt, P. C. A. Bruijnincx, B. M. Weckhuysen, *J. Am. Chem. Soc.* **2017**, *139*, 13632–13635.
[21] A. Zürner, J. Kirstein, M. Döblinger, C. Bräuchle, T. Bein, *Nature* **2007**, *450*, 705–708.
[22] N. M. Andoy, X. Zhou, E. Choudhary, H. Shen, G. Liu, P. Chen, *J. Am. Chem. Soc.* **2013**, *135*, 1845–1852.
[23] E. Debroye, J. Van Loon, X. Gu, T. Franklin, J. Hofkens, K. P. F. Janssen, M. B. J. Roeffaers, *Part. Part. Syst. Charact.* **2016**, *33*, 412–418.
[24] J. Van Loon, K. P. F. Janssen, T. Franklin, A. V. Kubarev, J. A. Steele, E. Debroye, E. Breynaert, J. A. Martens, M. B. J. Roeffaers, *ACS Catal.* **2017**, *7*, 5234–5242.
[25] M. H. F. Kox, A. Mijovilovich, J. J. H. B. Sättler, E. Stavitski, B. M. Weckhuysen, *ChemCatChem* **2010**, *2*, 564–571.
[26] G. T. Whiting, F. Meirer, D. Valencia, M. M. Mertens, A. Bons, B. M. Weiss, P. A. Stevens, E. De Smit, B. M. Weckhuysen, *Phys. Chem. Chem. Phys.* **2014**, *16*, 21531–21542.
[27] M. B. J. Roeffaers, G. De Cremer, J. Libeert, R. Ameloot, P. Dedecker, A.-J. Bons, M. Bückins, J. A. Martens, B. F. Sels, D. E. de Vos, J. Hofkens, *Angew. Chem. Int. Ed.* **2009**, *48*, 9285–9289; *Angew. Chem.* **2009**, *121*, 9449–9453.
[28] P. Dedecker, S. Duwé, R. K. Neely, J. Zhang, *J. Biomed. Opt.* **2012**, *17*, 1–5.
[29] T. Dertinger, R. Colyer, G. Iyer, S. Weiss, J. Enderlein, *Proc. Natl. Acad. Sci. USA* **2009**, *106*, 22287–22292.
[30] R. A. Beyerlein, C. Choi-feng, J. B. Hall, B. J. Huggins, G. J. Ray, *Top. Catal.* **1997**, *4*, 27–42.
[31] C. Choifeng, J. B. Hall, B. J. Huggins, R. A. Beyerlein, *J. Catal.* **1993**, *140*, 395–405.
[32] L. R. Aramburo, Y. Liu, T. Tyliszczak, F. M. F. De Groot, J. C. Andrews, B. M. Weckhuysen, *ChemPhysChem* **2013**, *14*, 496–499.
[33] C. Sprung, B. M. Weckhuysen, *Chem. Eur. J.* **2014**, *20*, 3667–3677.

Manuscript received: September 19, 2017
Version of record online: November 20, 2017

